NIH Public Access
Author Manuscript
Alzheimers Dement. Author manuscript; available in PMC 2011 March 1.

Published in final edited form as:
Alzheimers Dement. 2010 March ; 6(2): 110–117. doi:10.1016/j.jalz.2009.06.002.

Characterization of tau fibrillization *in vitro*

Shaohua Xu[#], **Kurt R. Brunden**, **John Q. Trojanowski**, and **Virginia M.-Y. Lee**[*]
The Center for Neurodegenerative Disease Research, Department of Pathology and Laboratory Medicine, and Institute on Aging, University of Pennsylvania School of Medicine, Philadelphia, PA

Abstract

Background—The assembly of tau proteins into paired helical filaments, the building blocks of neurofibrillary tangles, is linked to neurodegeneration in Alzheimer's disease and related tauopathies. A greater understanding of this assembly process could identify targets for the discovery of drugs to treat Alzheimer's disease and related disorders. Using recombinant human tau, we have delineated events leading to the conversion of normal soluble tau into tau fibrils

Methods—Atomic force microscopy and transmission electron microscopy methodologies were utilized to determine the structure of tau assemblies that formed when soluble tau was incubated with heparin for increasing lengths of time.

Results—Tau initially oligomerizes into spherical nucleation units of 18–21 nm diameter that appear to assemble linearly into nascent fibrils. Among the earliest tau fibrils are species that resemble a string of beads formed by linearly aligned spheres that with time seem to coalesce to form straight and twisted ribbon-like filaments, as well as paired-helical filaments similar to those found in human tauopathies. An analysis of fibril cross-sections at later incubation times revealed three fundamental axial structural features.

Conclusions—By monitoring tau fibrillization, we show that different tau filament morphologies co-exist. Temporal changes in the predominant tau structural species suggest that tau fibrillization involves the generation of structural intermediates, resulting in the formation of tau fibrils with verisimilitude to their authentic human counterparts.

Keywords

Alzheimer's disease; tauopathy; amyloid; tangles; neurodegeneration

1. Background

The first ultrastructural characterizations of Alzheimer's disease (AD) neurofibrillary tangles (NFTs) were reported nearly fifty years ago (1–3), and these early electron microscopic (EM) studies noted that NFTs were composed principally of paired helical filaments (PHFs). Subsequently, tau was suggested to be a major building block of NFTs and PHFs (4–8), but it

© 2009 Elsevier Inc. All rights reserved.

*Address correspondence to: Dr. Virginia M.-Y. Lee, Center for Neurodegenerative Disease Research, Department of Pathology and Laboratory Medicine, HUP, 3rd Floor Maloney Building, University of Pennsylvania School of Medicine, 3600 Spruce Street, Philadelphia, PA 19104, Tel: (215)-662-6427, Fax: (215)-349-5909, VMYLEE@mail.med.upenn.edu.
[#]Current Address: Space Life Sciences Laboratory, Kennedy Space Center, FL; Biological Sciences Department, Florida Institute of Technology, Melbourne, FL

Publisher's Disclaimer: This is a PDF file of an unedited manuscript that has been accepted for publication. As a service to our customers we are providing this early version of the manuscript. The manuscript will undergo copyediting, typesetting, and review of the resulting proof before it is published in its final citable form. Please note that during the production process errors may be discovered which could affect the content, and all legal disclaimers that apply to the journal pertain.

NIH-PA Author Manuscript
NIH-PA Author Manuscript
NIH-PA Author Manuscript

NIH-PA Author Manuscript

NIH-PA Author Manuscript

NIH-PA Author Manuscript

was not until 1991 that abnormally phosphorylated tau proteins were shown unequivocally to form PHFs in AD NFTs (9). Indeed, NFTs as well as glial tangles and neuropil threads composed of filamentous tau aggregates are signature lesions of several neurodegenerative disorders that are referred to collectively as tauopathies (for reviews, see 10–12), and the discovery of multiple tau gene mutations pathogenic for familial tauopathies known as frontotemporal dementia with parkinsonism linked to chromosome 17 (FTDP-17) provided compelling evidence that tau abnormalities cause neurodegeneration (12). Moreover, a causative role for tau pathologies in neurodegenerative disorders has been strongly supported by the development of tau transgenic animals that model human tauopathies (10,13).

Tau was first identified as a microtubule (MT)-associated protein that binds to and stabilizes MTs (14). In the normal adult human brain, six tau isoforms ranging from 352 to 441 amino acid residues in length are generated by alternative splicing from the same gene and are expressed mainly in neurons (6,15). These isoforms may have different affinities for MTs, as well as different propensities to form filamentous inclusions (12). When tau is abnormally phosphorylated and fibrillizes into PHFs, the protein cannot perform its normal functions, which leads to impaired MT stability and disrupted axonal transport that likely contributes to neurodegeneration (reviewed in 10,12,16).

Pathological tau fibrils show diverse morphologies in diseased brains, where transmission EM (TEM) images typically reveal PHFs in AD NFTs or neuropil threads, although straight filaments (SFs) and twisted ribbons (TRs) are also seen. Additional morphological variants of tau fibrils have been observed in other tauopathies such as progressive supranuclear palsy (PSP), corticobasal degeneration (CBD), Pick's disease and FTDP-17 syndromes (as reviewed in 12 and illustrated by 1,17–21). There is still an incomplete understanding of the sequence of events leading to tau fibrillization, and it is unclear how the different structural variants of tau fibrils arise or if these variants (e.g. PHFs, SFs, TRs) are inter-convertible (17,22–24).

Tau proteins fibrillize efficiently *in vitro* into β-pleated sheet structures with biochemical and biophysical properties of amyloid fibrils, but they do so only in the presence of negatively charged co-factors such as heparin, RNA or DNA (23,25). The kinetic profile of tau fibrillization *in vitro* generally resembles that of other amyloid proteins, with a lag phase during which time nucleating units are believed to be formed followed by rapid fibril growth. This has led to several proposed "nucleation-elongation" models of tau fibril assembly (26–29). In addition, an alternative linear colloidal aggregation model has been proposed for tau in which the protein forms colloidal spheres that serve as nucleation units which, through charge-dipole and dipole-dipole interactions, go on to form linear fibers (30,31). Recent studies in which the assembly of tau fibrils was examined by scanning TEM or atomic force microscopy (AFM) provide support for a colloidal assembly model (32–34). These experiments revealed higher order tau structures that appeared to result from the stepwise association of core oligomeric units of ~15–25 nm in size that were suggested to be comprised of an assembly of ~15 (32) to ~40 tau monomers (33). However, these two putative mechanisms of tau fibrillization remain to be proven and are not mutually exclusive.

Since the elucidation of specific tau fibrillization pathways may provide insights into disease mechanisms and reveal potential therapeutic targets for drug discovery, here we used TEM and AFM to further dissect the conversion of soluble recombinant human tau protein into a number of intermediates that culminate in mature tau fibrils. Consistent with recent findings, we identify early spherical nucleation units (SNUs) that appear to align to form linear assemblies. At later times, fibers with diverse morphologies are found that may be derived from assembled SNUs. Thus, the studies described here further define the formation of tau fibrils from soluble monomers.

NIH-PA Author Manuscript

NIH-PA Author Manuscript

NIH-PA Author Manuscript

2. Methods

2.1 Tau40 preparation and fibril formation

Recombinant Tau40 protein was generated in *E.Coli* as described previously, with isolation by FPLC using a Mono-S column (35) and protein concentration determined by the BCA method. Tau40 is the largest tau isoform, containing both of the alternatively spliced amino terminal exons as well as four MT binding repeats (4R-tau). Fibrillization was initiated by incubating samples of recombinant Tau40 with heparin at a molar ratio of 1:2 in 100 mM sodium acetate, pH 7.4 with agitation at 1000 rpm at 37°C as described (36). Aliquots of the reaction mixture were removed at various time points and stored at −70°C for analysis. The initial concentration of Tau40 was 44 μM (for rapid fibrillization) or 22 μM (for slower fibrillization).

2.2 AFM imaging

A multi-mode AFM (Bioscope IIIa, Digital Instruments, Santa Barbara, CA) was used in these experiments. For contact mode, imaging generally began in a 5×5 nm^2 area. When stable images were obtained, the scanning force was minimized by a reduction of the set point voltage, and the scanning area was increased to the desired size. Long and narrow-legged standard Si_3N_4 cantilever tips were used for contact mode when imaging dry, while short and narrow-legged cantilevers were used in tapping mode when imaging in solution. Only contact mode was used when imaging dry, and tapping mode was utilized only when imaging wet. The tapping mode wet imaging was performed largely to confirm results obtained from dry contact mode imaging, including verification that the particles observed in dry imaging were not due to salt deposits. The imaging was conducted at 3–5% off the resonance frequency of the cantilever. The raw data were plane-fit and particle height was measured with the NanoScope III off-line data analysis program. To prepare specimens for AFM imaging, an aliquot of diluted Tau40 protein that had been captured at various times after heparin addition was dispensed to form a layer of 1 cm in diameter on mica. The specimen was incubated for 5 min for absorption of the protein to the surface of the mica at room temperature. For imaging in solution, the specimen was then mounted directly onto the AFM sample stage. An additional 50 μl buffer solution was added before imaging. For imaging dry, a mica disk was rinsed with a few drops of water and dried in air.

2.3 TEM imaging

Tau fibrils and fibrillization intermediates were captured at various times after incubation with heparin, adsorbed onto 200-mesh formvar-coated copper grids, stained with 1% uranyl acetate, and imaged with a Joel 1010 TEM (Peabody, MA) as described (30). Images were captured with a Hamamatsu (Bridgewater, MA) digital camera using AMT (Danvers, MA) software. The dimensions of the particles and fibers were measured and recorded in Photoshop. Structural features in a TEM image were measured and compared to the scale bar on the image for the lateral dimensions.

Cross-sections of tau fibrils were produced from preparations embedded in Epon. Samples harvested at late stages of fibrillization were fixed with glutaraldehyde (1%) for 20 min and pelleted. Pre-heated low melting agarose (10 μl) was then mixed with these preparations. After rinsing with sodium cacodylate (0.1 M, three times), samples were stained with uranyl acetate (2%, 30 min) and dehydrated with ethanol (a total of 50 min in increasing concentrations of ethanol from 50 to 100%). Samples were then rinsed with 1:1 ethanol/propylene oxide (PO) followed by a rinse with a propylene 100% PO solution before embedding in PO:Epon overnight at 4°C. This was followed by embedding in full Epon at 60°C. Ulta-thin sections were cut and placed on a carbon grid that was stained with uranyl acetate (7% in 50% ethanol) and rinsed first with ethanol (50%) and then five times with water.

NIH-PA Author Manuscript

NIH-PA Author Manuscript

NIH-PA Author Manuscript

3. Results

3.1 Formation of tau spherical nucleation units (SNUs) and their linear assembly

Tau40 was isolated as described in "Methods" and after incubation with heparin was found to rapidly oligomerize within one day into spheres that could be imaged by AFM and which are referred to here as SNUs (Fig. 1A). While we use the term "spherical nucleation units", it is possible that smaller nucleation assemblies are formed that are not readily observed but which serve as precursors of SNUs. Some of the SNUs formed short arrays of linear assembled nucleation units (see Fig. 1), and both individual SNUs and those arrayed into assemblies were similar in size with diameters of 18.5 ± 3.8 nm (n = 573). The appearance and size of the SNUs is in close agreement to the granular structures recently reported by Maeda et al. (33) and these authors reported that these oligomers adopt a conformation that allows thioflavine T binding, suggesting the presence of β-sheet secondary structure.

We found that nascent fibril formation from SNUs could be influenced by the concentration of tau, and while we made no attempts to precisely define fibrillization kinetics we noted that reducing the tau concentration slowed assembly rates but did not alter the ultimate formation of SNUs or protofibrils, SNUs appeared to be more abundant at early time points of incubation (i.e., days 1–9) and decreased progressively over 3 weeks of incubation concomitant with an increased abundance of long tau fibrils (Fig. 1B). For example, the number of SNUs after 9 days of incubation (Fig. 1A) is ~5-fold greater than after 18 days of incubation (Fig. 1B), whereas the total fiber length at 18 days was found to be 5-fold that observed at 9 days.

TEM images revealed nascent tau fibrils to be composed of linear arrays of SNUs resembling beads on a string (Fig. 2A), and SNUs in small assemblies or in larger arrays appeared tightly packed with smooth surfaces (Fig. 2A & 2B). Quantitative analysis of TEM images indicated the diameters of the SNUs at this stage to be 21.1 ± 2.9 nm (n = 81), ranging between 14.0 and 26.6 nm. The differences in the diameters of SNUs measured in TEM and AFM images most likely reflect the different methodologies used to image them and the compression effects observed in AFM images. The diameters of the SNUs in protofibrils were similar to the diameters of the unassembled ones, suggesting that SNUs are the initial building blocks of nascent tau fibrils. Representative short fibrils made of discrete numbers of SNUs are illustrated in Figure 2B.

3.2 Twisted protofibrils and multi-striated ribbons

Striated ribbons were present in samples at 9 to 18 days after aggregation was initiated (Fig. 3A), and their appearance was accompanied by what appeared to be a merging or dissolution of the SNUs and the formation of striations within individual fibrils with the appearance of a "fluffy" material wrapping around the fibrils. A previous study (34) also noted the presence of a fluffy coating of tau40 filaments that was not observed in fibrils formed from truncated tau, and these authors suggested that this material results from the loose packing of hydrophilic regions of tau.

While it is difficult to define the exact mechanism of striated ribbon genesis, TEM images such as those shown in Fig. 3A suggest that the boundaries between the assembled SNUs within initial protofibrils erode during ribbon formation due to their presumptive annealing and changes in the bead-to-bead distance.

3.3 Multi-striated ribbons and ribbons with center depressions

Continued incubation of mixtures enriched in striated ribbons resulted in two types of ribbon-like structures that were designated multi-striated ribbons (MSRs) and ribbons with center depressions (RCDs). RCDs and MSRs appeared similar in structure (Fig. 3B–C) to tau

NIH-PA Author Manuscript

NIH-PA Author Manuscript

NIH-PA Author Manuscript

aggregates isolated from brains with sporadic Pick's disease (21) and CBD (32). These ribbons existed in various widths ranging from 5 to 25 nm and in lengths ranging from 20 nm to a few microns. RCDs appeared to be more frequent than MSRs, and the center depression existed on both sides of ribbons, as revealed by ribbons with a 180° twist. The two leaflets or filaments sandwiching the center depression were similar in length and width, although in some instances one leaflet was shorter in length. Like the filaments observed in Pick's disease and CBD, there were some instances where the leaflets of RCDs appeared to be separating into two single filaments. The observations here indicate that ribbons were twisted to a highly variable degree. In the absence of twisting, RCDs appeared as two pale parallel lines of equal length and width that may represent aligned filaments. Some segments resembled SFs and the diameter of these SF-like segments was ~7.2 ± 0.6 nm (n=20).

3.4 Formation of twisted ribbons (TRs) and PHF-like Structures

At later stages of incubation, structures resembling PHFs, as well as SFs and TRs, were observed that mimicked those seen in authentic human tauopathies (Fig. 4A–B). Most tau fibrils showed some degree of twisting, and the main difference between the MSRs and the PHF-like structures appeared to be the degree or extent of twisting. The PHF-like structures showed a periodicity of 82.7 ± 4.6 nm (n=12), and the width of the untwisted region of these filaments was 23.6 ± 3.1 nm (n=23), ranging from 18.9 to 28.9, while the width of the twisted region was 12.9 ± 1.3 nm (n=12), ranging from 10.9 to 14.2 nm. Ribbons with irregular twists also were present with a periodicity shorter or longer than 82.7 nm. The width of ribbons with a modest degree of twisting was 18.4 ± 1.7 nm (n=16), ranging from 16.8 to 22.1 nm, so the width of the untwisted region of a PHF-like structure was 28.2% larger than that of ribbons with a modest degree of twisting.

We analyzed tau fibrils captured at late stages of fibrillization by examining thin sections of these fibrils embedded in Epon by TEM. Cross-sectional analyses revealed three major structural features: a disk, an ellipsoid, and a dumbbell-shape (Fig. 4C). The variations in cross-sectional shape are likely caused by the different arrangements of the strands shown in Figs. 4A–B, with the dumbbell shape perhaps representing paired filaments. A schematic that takes into account the various tau structural variants described herein with a possible chronology of appearance is shown in Fig. 5. Fundamental to the formation of the various tau filaments is the initial stepwise assembly of SNUs into higher order structures that then undergo structural transitions.

4. Discussion

We have used AFM and TEM to analyze the progressive fibrillization of recombinant human tau protein (Tau40) in an *in vitro* assay system that results in the production of tau fibrils similar to those seen in authentic human AD and related neurodegenerative tauopathies. The nature of these methodologies limits our ability to make precise quantitative statements about the relative abundance of structures as a function of incubation time, as we cannot exclude the possibility that certain structures are under-represented due to poor adherence to TEM grids. Rather, these studies enabled us to characterize the temporal aggregation of monomeric tau into multimeric intermediate structures and ultimately into tau filaments, including mature PHFs and SFs. Based on the chronological appearance of these intermediates, we hypothesize a sequence of events in the fibrillization of tau that begins with an early aggregation stage during which time SNUs form and subsequently align as linear arrays. This initial phase of tau fibrillization is then followed by a stage that is heralded by the generation of striated ribbons and MSRs, culminating in the complete fibrillization of tau and the generation of fully formed tau amyloid fibrils (summarized in Fig. 5).

NIH-PA Author Manuscript

NIH-PA Author Manuscript

NIH-PA Author Manuscript

The observation that SNUs combine and ultimately coalesce and/or melt together is consistent with recent STEM and AFM studies of tau fibrillization (32,33). After SNUs have coalesced, we found that tau filaments of different morphologies such as MSRs and RCDs arise and are found to co-exist in the same reaction mixtures, although there is in general a temporal maturation to TR, SF and PHF structures. This suggests that tau filaments undergo a series of conformational rearrangements before fibrillization is fully complete. Indeed, our cross-sectional analyses of tau fibrils indicate that there are at least three distinct axial morphologies of the mature tau filaments. Furthermore, if the various morphologies assumed by tau amyloid fibrils reflect a degree of strand twisting and/or associationc, which may remain malleable, then the morphological distinct end-products of the tau fibrillization pathways described here may be inter-convertible.

Interestingly, there are differences in the tau fibril morphology found within different human tauopathies. For example, classical PHFs, which are comprised of all 6 tau isoforms, are found predominantly in NFTs of AD (12,37). On the other hand, SFs and PHFs are found in CBD and PSP, and are comprised primarily of tau isoforms with four MT binding repeats (4R-tau) rather than 3R-tau. Finally, TRs are more abundant in FTDP-17 with *tau* gene mutations (12, 37,38). The exact reason for the diverse morphologies of tau fibrils in these different tauopathies is not known, but it is unlikely that they are due to isoform composition since both SFs in CBD/PSP and TRs in FTDP-17 are comprised primarily of 4R-tau (12,37,38). Moreover, as demonstrated here, all of these tau fibril morphologies can be formed *in vitro* from Tau40 (4R-tau). Thus, mechanisms or factors other than the ratio of 3R-tau to 4R-tau isoforms are likely to be responsible for inducing tau fibrils to assume the different morphologies of SFs, PHFs and TRs seen in the brains of patients with taupathies.

Unlike other amyloidogenic proteins or peptides (e.g. α-synuclein, prions and Aβ) that assemble into amyloid fibrils *in vitro* in the absence of co-factors, tau fibrillization requires concomitant incubation with heparin or other polyanions to initiate tau fibrillogenesis (36, 39). The mechanism whereby such co-factors initiate tau fibril formation is not well understood. Heparin or other polyanions may be required for tau nucleation by acting through one or more mechanisms, including 1) neutralizing positive charges on tau molecules and thereby reducing electrostatic repulsion that might retard aggregation; 2) binding to tau, thereby unfolding the molecule and exposing hydrophobic regions that are needed for nucleation to proceed or by bringing multiple tau molecules into close proximity or; 3) promoting hydrophobic interactions by stabilizing H-bonds of surrounding water molecules. These uncertainties notwithstanding, one of the earliest stages in the fibrillization of tau appears to be the formation of oligomeric SNUs, and we estimate that the number of tau molecules in each SNU to be ~74 ($n= 0.74*4/3\pi R^3/V_\tau$ where R is the radius of the SNUs and V_τ is the calculated volume of the individual tau molecule; see 40). This is somewhat higher than a previous estimate of ~40 tau monomers within core tau oligomeric structures (33) and this discrepancy may result from the different methodologies used in measuring the diameter of the SNUs.

AFM and TEM images indicate that SNUs formed in the early stages of the tau fibrillization reaction align to form the initial fibrils. These data support a linear colloidal aggregation model (31) and are consistent with recent observations by Maeda et al. (33). A similar alignment of spherical units was also reported in a hanging drop assembly of tau fibrils, although the fibrils formed by this method differed from those obtained by the same researchers when they utilized an arachidonic acid-mediated tau assembly reaction (32). The colloidal aggregation model contrasts with the more classical nucleation-elongation theory of tau fibril formation in which fibril growth is postulated to proceed by the addition of monomers to a nucleating core. It is possible that the assembly pathways leading to tau fibril formation are greatly influenced by the assay conditions employed, as these often vary considerably in the choice of anionic co-

NIH-PA Author Manuscript

NIH-PA Author Manuscript

NIH-PA Author Manuscript

factor, tau concentrations, buffers and mixing conditions. For example, tau fibril assembly reactions that are continually mixed may favor a colloidal pathway over a nucleation-elongation mechanism. Conversely, we and others have found that tau fibrillization reactions can be greatly accelerated by the addition of fully mature fibrils (29,41), and the introduction of these fibrillar nucleation scaffolds may drive further growth by elongation from existing fibril ends in a process that disfavors a colloidal pathway. It is also possible that multiple assembly pathways can occur simultaneously. Thus, while we observed intermediate structures that suggested a linear association of SNUs, we cannot conclude that this was the only pathway of fibrillization in our reactions. Finally, while *in vitro* studies of tau fibrillization provide useful information, it remains unknown which reaction conditions and assembly pathway(s) most closely mimic those that occur in neurons.

Although there are caveats to the interpretation of tau assembly *in vitro*, the information obtained from such studies may nonetheless provide potential therapeutic targets for neurodegenerative tauopathies. Based on the sequence of tau fibrillization described herein, it would seem that either inhibiting the assembly of tau monomers into SNUs, or preventing the stepwise association of SNUs that results in nascent fibril formation, might be a tractable approach to reducing the formation of tau inclusions. Whether such protein-protein interactions can be prevented by classical small molecule drugs remains to be determined.

Acknowledgments

This work was supported by grants from the National Institutes of Health (AG-09215 and AG-17586), the Oxford Foundation, and the Marian S. Ware Alzheimer Program of the University of Pennsylvania. Dr. Xu also recognizes financial support from the Brevard Community Foundation. The authors thank A. Crowe and R. Miller III for the preparation of tau proteins, and Dr. D.P. Chen of Rush Medical School and Dean Astumin of University of Maine for helpful discussions. Dr. Peter Davies kindly provided access to the AFM facility at the Penn Institute of Medicine and Engineering, and TEM was performed in the Penn Morphology Core. VMYL is the John H. Ware 3rd Professor for Alzheimer's Disease Research and JQT is the William Maul Measy-Truman G. Schnabel Jr. M.D. Professor of Geriatric Medicine and Gerontology.

Abbreviations

AD	Alzheimer's disease
AFM	Atomic force microscopy
BMSRs	Beaded multi-striated ribbons
EM	Electron microscopy
NFTs	Neurofibrillary tangles
PHFs	Paired helical filaments
RCDs	Ribbons with a center depression
SFs	Straight filaments
SNUs	Spherical nucleation units
TEM	Transmission electron microscopy
TRs	Twisted ribbons

References

1. Kidd M. Paired helical filaments in electron microscopy of Alzheimer's disease. Nature 1963;197:192–193. [PubMed: 14032480]

NIH-PA Author Manuscript NIH-PA Author Manuscript NIH-PA Author Manuscript

2. Kidd M. Alzheimer's disease--an electron microscopical study. Brain 1964;67:307–320. [PubMed: 14188276]
3. Terry RD. The fine structure of neurofibrillary tangles in Alzheimer's disease. J Neuroapth Exper Neurol 1963;22:629–642.
4. Brion JP, Passareiro H, Nunez J, Flament-Durand J. Neurofibrillary tangles of Alzheimer's disease: an immunohistochemical study. Arch Biol 1985;96:229–235.
5. Brion JP, Flament-Durand J, Dustin P. Alzheimer's disease and tau proteins. Lancet 1986;2:1098. [PubMed: 2877247]
6. Goedert M, Spillantini MG, Jakes R, Rutherford D, Crowther RA. Multiple isoforms of human microtubule-associated protein tau: sequences and localization in neurofibrillary tangles of Alzheimer's disease. Neuron 1989;3:519–526. [PubMed: 2484340]
7. Grundke-Iqbal I, Iqbal K, Tung YC, Quinlan M, Wisniewski HM, Binder LI. Abnormal phosphorylation of the microtubule-associated protein tau in Alzheimer cytoskeletal pathology. Proc Natl Acad Sci USA 1986;83:4913–4917. [PubMed: 3088567]
8. Wood JG, Mirra SS, Pollock NJ, Binder LI. Neurofibrillary tangles of Alzheimer disease share antigenic determinants with the axonal microtubule-associated protein tau. Proc Natl Acad Sci USA 1986;83:4040–4043. [PubMed: 2424015]
9. Lee VM-Y, Balin BJ, Otvos L, Trojanowski JQ. A68: a major subunit of paired helical filaments and derivatized forms of normal tau. Science 1991;251:675–678. [PubMed: 1899488]
10. Ballatore C, Lee VM-Y, Trojanowski JQ. Tau mediated neurodegeneration in Alzheimer's disease and related disorders. Nature Rev Neurosci 2007;8:663–672. [PubMed: 17684513]
11. Forman MS, Trojanowski JQ, Lee VM-Y. Neurodegenerative diseases: A decade of discoveries paves the way for therapeutic breakthroughs. Nat Med 2004;10:1055–1063. [PubMed: 15459709]
12. Lee VM-Y, Goedert M, Trojanowski JQ. Neurodegenerative tauopathies. Annu Rev Neurosci 2001;24:1121–1159. [PubMed: 11520930]
13. Lee VM-Y, Kenyon TK, Trojanowski JQ. Transgenic animal models of tauopathies. Biochem Biophys Acta 2005;1739:251–259. [PubMed: 15615643]
14. Weingarten MD, Lockwood AH, Hwo SY, Kirschner MW. A protein factor essential for microtubule assembly. Proc Natl Acad Sci USA 1975;72:1858–1862. [PubMed: 1057175]
15. Lee G, Cowan N, Kirschner M. The primary structure and heterogeneity of tau protein from mouse brain. Science 1988;239:285–288. [PubMed: 3122323]
16. Trojanowski JQ, Smith AB 3rd, Huryn D, Lee VM-Y. Microtubule stabilizing drugs for therapy of Alzheimer's disease and other neurodegenerative disorders with axonal transport impairments. Expert Opin Pharmacother 2005;6:683–686. [PubMed: 15934894]
17. Crowther RA, Wischik CM. Image reconstruction of the Alzheimer paired helical filament. EMBO J 1985;4:3661–3665. [PubMed: 2419127]
18. Ksiezak-Reding H, Morgan K, Mattiace LA, Davies P, Liu WK, Yen SH, Weidenheim K, Dickson DW. Ultrastructure and biochemical composition of paired helical filaments in corticobasal degeneration. Am J Pathol 1994;145:1496–1508. [PubMed: 7992852]
19. Reed LA, Schmidt ML, Wszolek ZK, Balin BJ, Soontornniyomkij V, Lee VM-Y, Trojanowski JQ, Schelper RL. The neuropathology of a chromosome 17-linked autosomal dominant parkinsonism and dementia. J Neuropathol Exp Neurol 1998;57:588–601. [PubMed: 9630238]
20. Shanker SK, Yanagihara R, Garruto RM, Grundke-Iqbal I, Kosik KS, Gajdusek DC. Immunocytochemical characterization of neurofibrillary tangles in amyotrophic lateral sclerosis and parkingsonism-dementia of Guam. Ann Neurol 1989;25:146–151. [PubMed: 2493213]
21. Zhuakareva V, Mann D, Pickering-Brown S, Uryu K, Shuck T, Shah K, Grossman M, Miller BL, Hulette CM, Feinstein SC, Tranjanowski JQ, Lee VM-Y. Sporadic Pick's disease: a tauopathy characterized by a spectrum of pathological τ isoforms in gray and white matter. Ann Neurol 2002;51:730–739. [PubMed: 12112079]
22. Crowther RA, Goedert M. Abnormal tau-containing filaments in neurodegenerative diseases. J Struct Biol 2000;130:271–279. [PubMed: 10940231]
23. Wilson DM, Binder LI. Free fatty acids stimulate the polymerization of tau and amyloid β peptides. Am J Pathol 1997;150:2181–2195. [PubMed: 9176408]

NIH-PA Author Manuscript NIH-PA Author Manuscript NIH-PA Author Manuscript

24. Yen S-H, Hutton M, DeTure M, Ko L-W, Nacharaju P. Fibrillogenesis of tau: insights from tau missense mutations in FTDP-17. Brain Pathol 1999;9:695–705. [PubMed: 10517508]
25. Goedert M, Jakes R, Spillantini MG, Hasegawa M, Smith MJ, Crowther RA. Assembly of microtubule associated protein tau into Alzheimer-like filaments induced by sulphated glycosaminoglycans. Nature 1996;383:550–553. [PubMed: 8849730]
26. Barghorn S, Mandelkow E. Toward a unified schede for the aggregation of tau into Alzheimer paired helical filaments. Biochemistry 2002;41:14885–14896. [PubMed: 12475237]
27. Chirita C, Congdon EE, Yin H, Kuret J. Triggers of full-length tau aggregationi: a role for partially folded intermediates. Biochemistry 2005;44:5862–5872. [PubMed: 15823045]
28. Congdon EE, Kim S, Bonchak J, Songrug T, Matzavinos A, Kuret J. Nucleation-dependent tau filament formation – the importance of dimerization and an estimation of elementary rate constants. J Biol Chem 2008;283:13806–13816. [PubMed: 18359772]
29. Friedhoff P, von Bergen M, Mandelkow EM, Davies P, Mandelkow E. A nucleated assembly mechanism of Alzheimer paired helical filaments. Proc. Natl. Acad. Sci. USA 1998;95:15712–15717. [PubMed: 9861035]
30. Xu S, Bevis B, Arnsdorf MF. The assembly of amyloidogenic yeast sup35 as assessed by scanning (atomic) force microscopy: an analogy to linear colloidal aggregation? Biophys J 2001;81:446–454. [PubMed: 11423427]
31. Xu S. Aggregation drives "misfolding" in protein amyloid fiber formation. Amyloid 2007;14:119–131. [PubMed: 17577685]
32. Ksiezak-Reding H, Wall JS. Characterization of paired helical filaments by scanning transmission electron microscopy. Microscopy Res Tech 2005;67:126–140.
33. Maeda S, Sahara N, Saito Y, Murayama M, Yoshiike Y, Kim H, Miyasaki T, Murayama S, Ikai A, Takashima A. Granular tau oligomers as intermediates of tau filaments. Biochemistry 2007;46:3856–3861. [PubMed: 17338548]
34. Von Bergen M, Barghorn S, Muller SA, Pickhardt M, Biernat J, Mandelkow E-M, Davies P, Aebi U, Mandelkow E. The core of tau-paired helical filaments studies by scanning transmission electron microscopy and limited proteolysis. Biochemistry 2006;45:6446–6457. [PubMed: 16700555]
35. Hong M, Zhukareva V, Vogelsberg-Ragaglia V, Wszolek Z, Reed L, et al. Mutation-specific functional impairments in distinct tau isoforms of hereditary FTDP-17. Science 1998;282:1914–1917. [PubMed: 9836646]
36. Giasson BI, Forman MS, Higuchi M, Golbe LI, Graves CL, Kotzbauer PT, Trojanowski JQ, Lee VM-Y. Initiation and synergistic fibrillization of tau and α-synuclein. Science 2003;300:636–640. [PubMed: 12714745]
37. Forman MS, Zhukareva V, Bergeron C, Chin SS-M, Grossman M, Clark C, Lee VM-Y, Trojanowski JQ. Signature tau neuropathology in gray and white matter of corticobasal degeneration. Am J Pathol 2002;160:2045–2053. [PubMed: 12057909]
38. Goedert M, Spillantini MG, Crowther RA, Chen SG, Parchi P, et al. Tau gene mutation in familial progressive subcortical gliosis. Nat Med 1999;5:454–457. [PubMed: 10202939]
39. Hasegawa M, Crowther RA, Jakes R, Goedert M. Alzheimer-like changes in microtubule-associated protein tau induced by sulfated glycosaminoglycans. Inhibition of microtubule binding, stimulation of phosphorylation, and filament assembly depend on the degree of sulfation. J Biol Chem 1997;272:33118–33124. [PubMed: 9407097]
40. Harpaz Y, Gerstein M, Chothia C. Volume changes on protein folding. Structure 1994;2:641–649. [PubMed: 7922041]
41. Aoyagi H, Hasegawa M, Tamaoka A. Fibrillogenic nuclei composed of P301L mutant tau induce elongation of P301L but not wild-type tau. J Biol Chem 2007;282:20309–20318. [PubMed: 17526496]

NIH-PA Author Manuscript

NIH-PA Author Manuscript

NIH-PA Author Manuscript

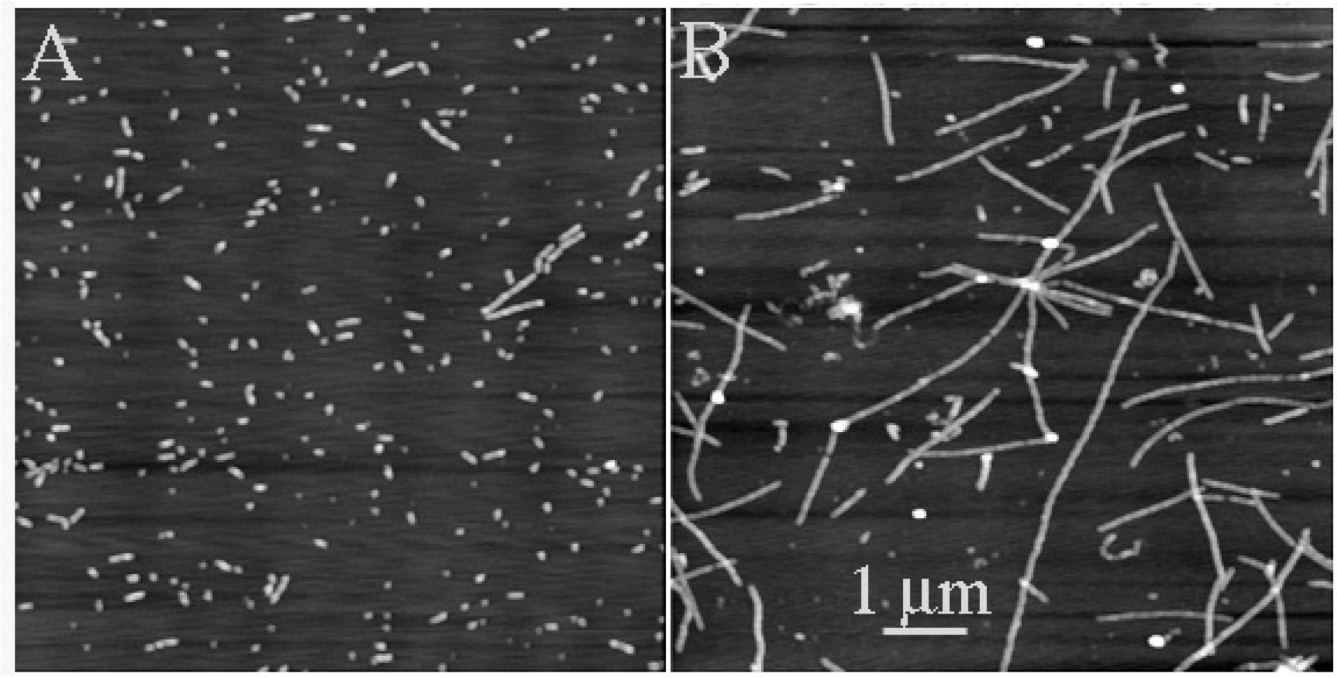

Figure 1. AFM imaging of Tau40 assembly into SNUs and their linear assembly

Tau40 mixtures that were incubated with heparin for 9 (Panel A) and 18 days (Panel B) were analyzed by contact mode AFM imaging in air using a long, narrow cantilever. Panel A reveals the presence of SNUs and short fibers that appear to be linear aggregates of SNUs. The density of SNUs decreases significantly by 18 days of incubation (Panel B), and fibrils have grown in length from day 9 to day 18. The scale bar is for both panels.

NIH-PA Author Manuscript

NIH-PA Author Manuscript

NIH-PA Author Manuscript

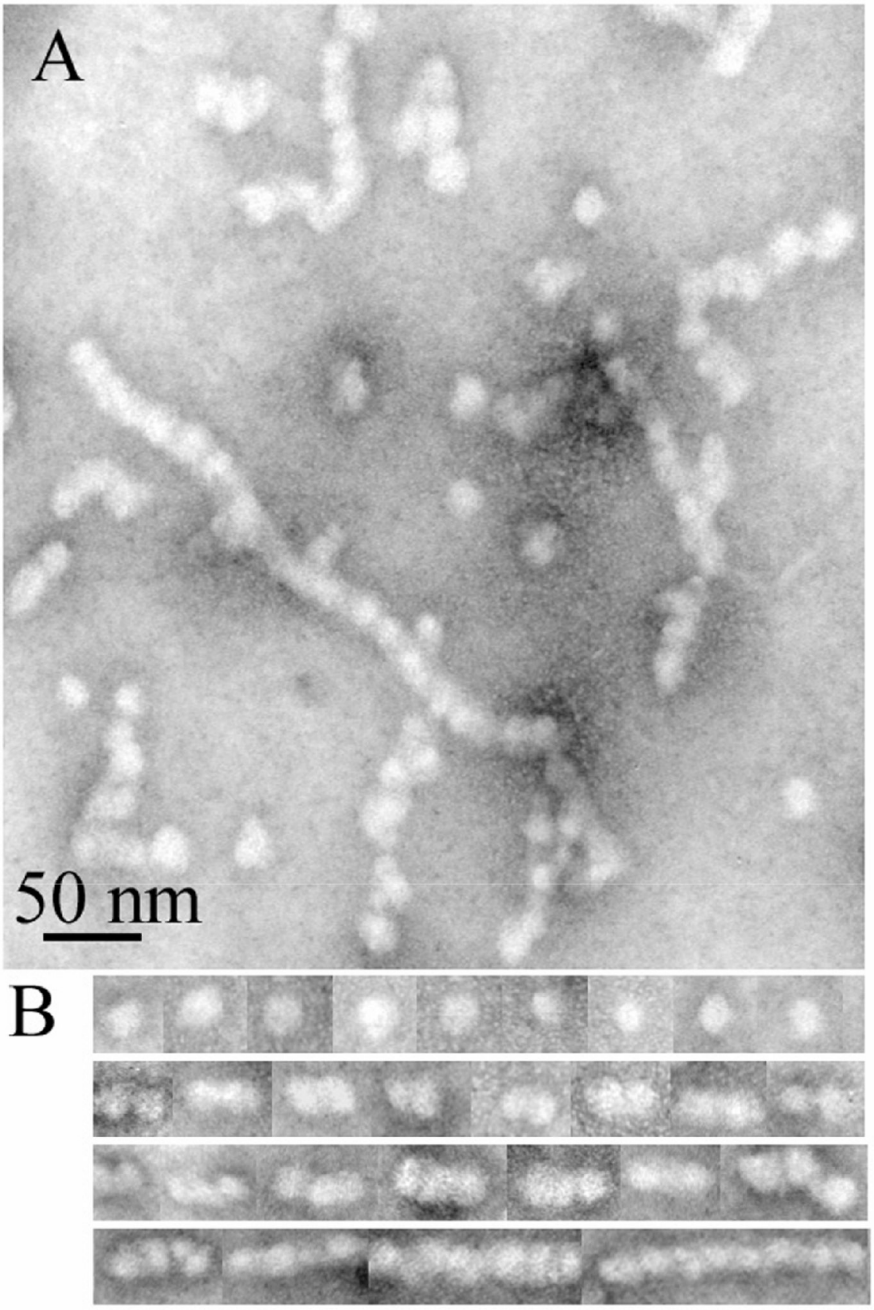

Figure 2. TEM image of SNUs and their assembly into protofibrils

A: EM image of a sample captured at day one showing the co-existence of both single and multiple SNUs strung together into linear assemblies. **B**: Assembly structures consisting of one, two, three, four, five, and more SNUs were selected from ten TEM images for illustration here. Magnifications in **B** are similar to **A**.

NIH-PA Author Manuscript

NIH-PA Author Manuscript

NIH-PA Author Manuscript

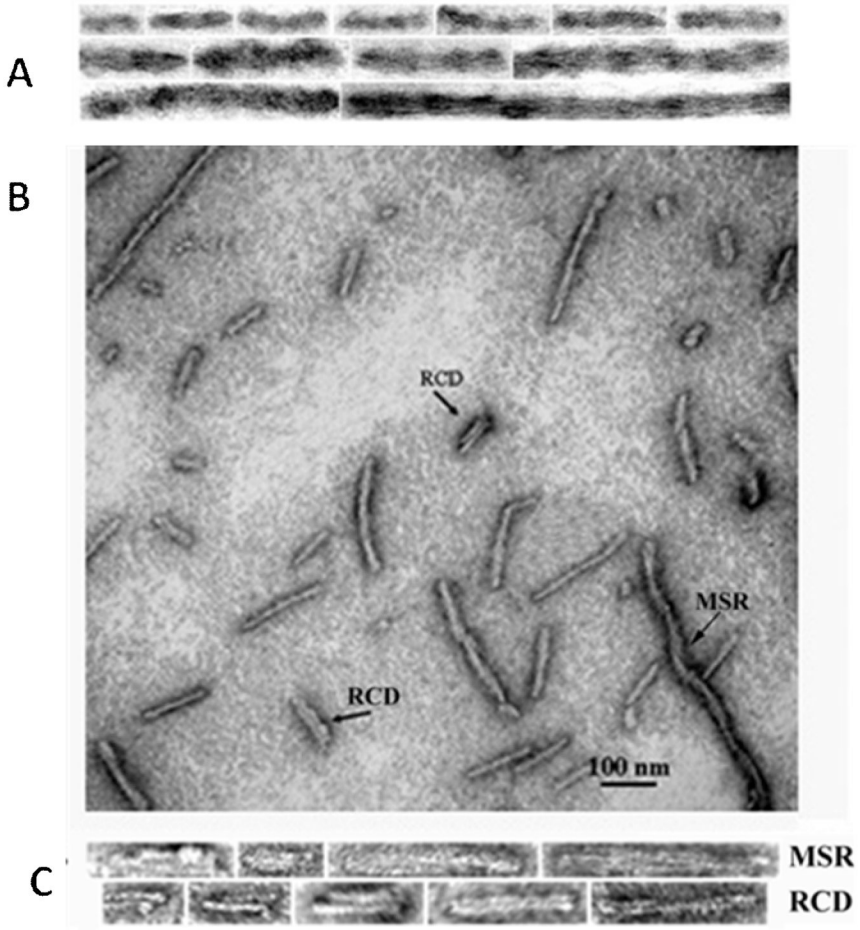

Figure 3. Characterization of advanced fibrils

TEM was performed for a specimen captured at day 9 to demonstrate more advanced Tau40 fibril intermediates. Multiple examples of striated ribbons selected from 20 different areas of multiple grids are presented in (**A**). Fluffy material representing perhaps the N- and C-terminus of Tau40 appears to wrap around the core of the fibrils. Samples captured at 21 days and beyond revealed two kinds of ribbons by TEM with different degrees of twisting (**B** and **C**). TEM image of RCDs with a dark line either on one side of the fiber or on both sides of fibers when found with a 180° twist, as well as MSRs (**B**). The distribution of MSRs and RCDs varied for different grids. Short ribbons with distinct characteristics are shown in **C**. For RCDs, the two leaflets were generally similar in length and width, while other ribbons varied in length and width. Twisting sometimes left one leaflet broken. MSRs were generally wider than RCDs. Magnifications in **C** are similar to **B** but photomicrographs in **C** are two-fold enlarged over those in **B**. Magnification in **A** is greater than **B** and **C** to allow greater visualization of fibrils.

NIH-PA Author Manuscript

NIH-PA Author Manuscript

NIH-PA Author Manuscript

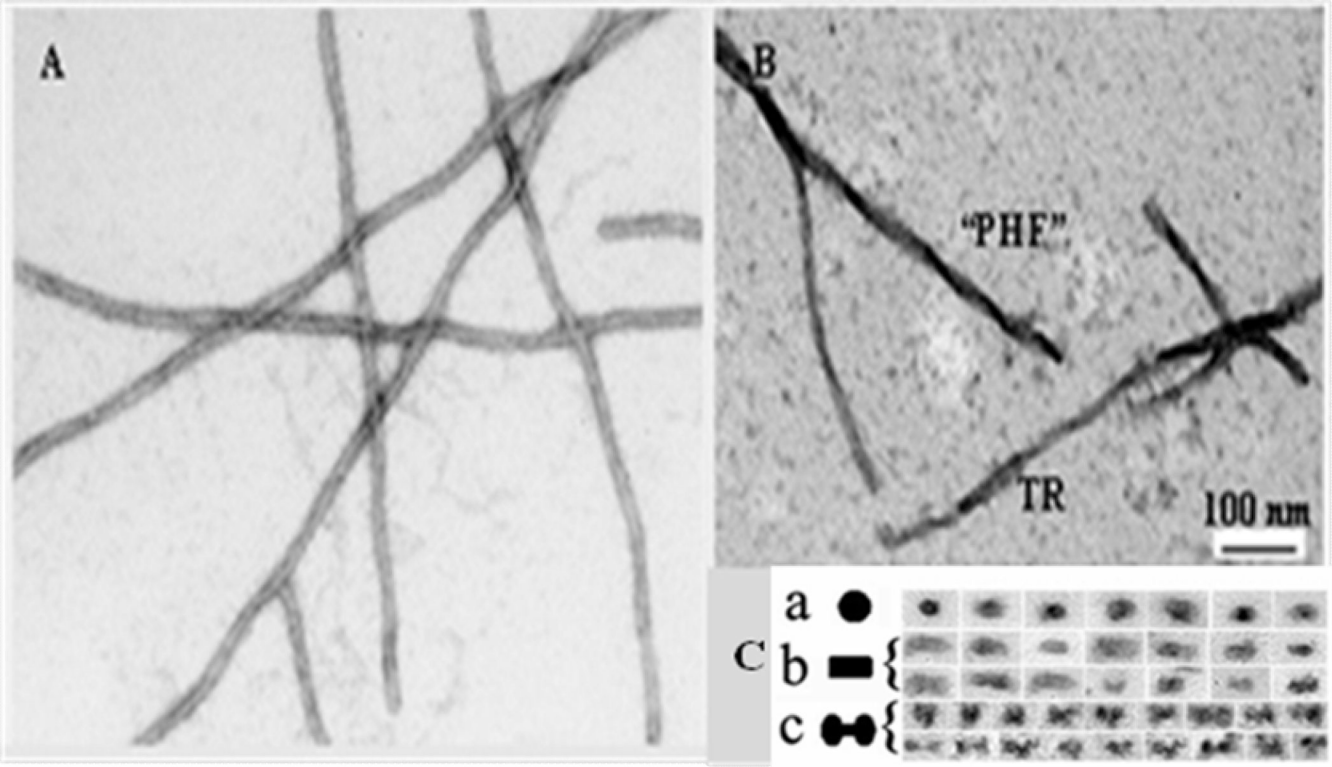

Figure 4. Tau fibrils with different morphologies

SFs (**A**), PHFs and TRs (**B**) can be detected in incubations of three weeks or more. Magnification in **A** is similar to **B**. Panel **C** represents cross-sections of fibrils captured after three weeks of incubation. Fibrils were trapped in a low-melting agarose gel and embedded with EPON. Thin sections were prepared and stained with uranyl acetate for TEM analysis. Cross-sections selected from ten TEM images from different areas of multiple grids are grouped according to the three major structural features identified: a disk (**a**), an ellipsoid (**b**), and a dumbbell-shape (**c**).

NIH-PA Author Manuscript

NIH-PA Author Manuscript

NIH-PA Author Manuscript

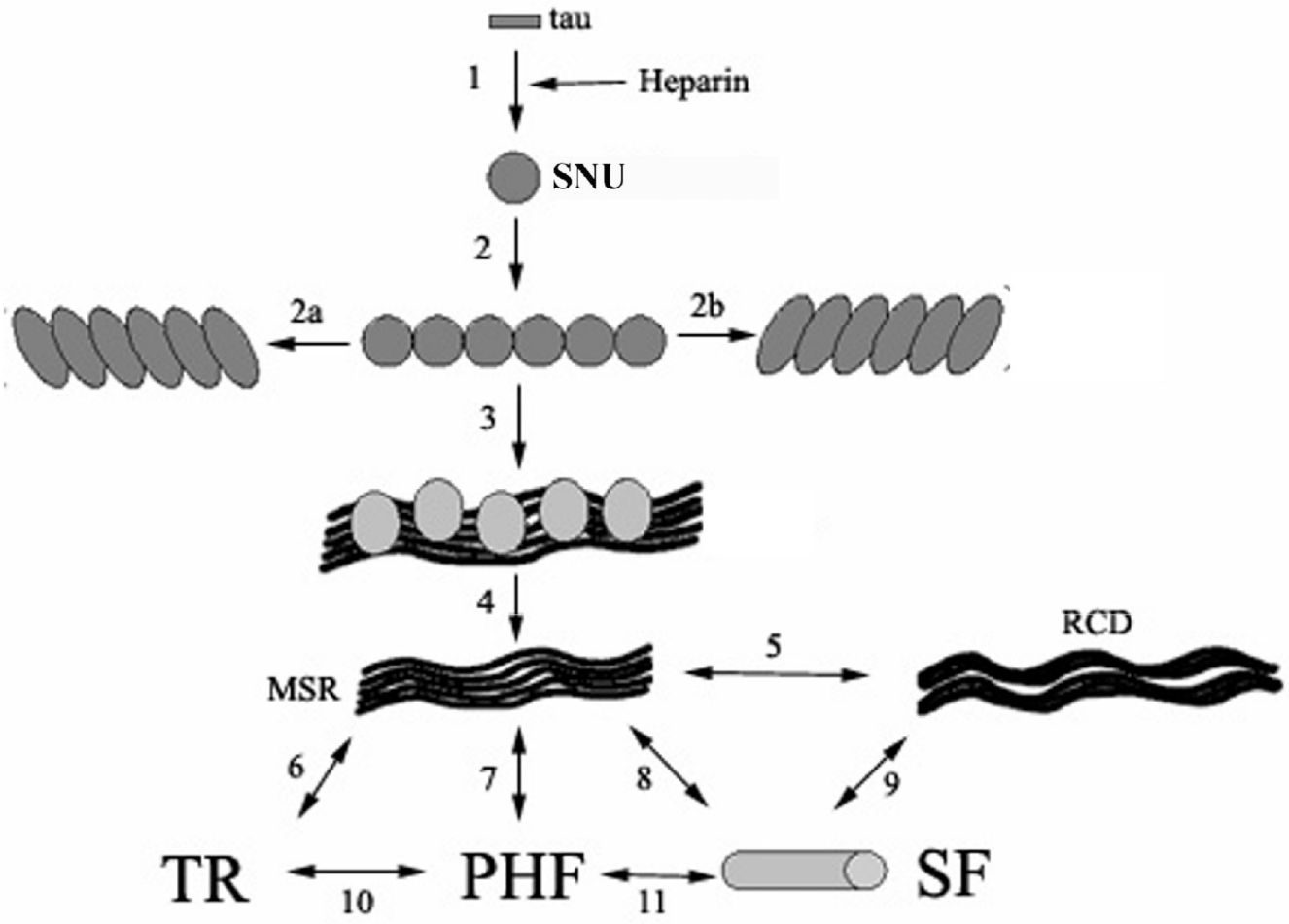

Figure 5. Schematic of hypothesized pathways of tau fibrillization

Tau40 (in the presence of heparin) oligomerizes to form SNUs (step 1), followed by the linear assembly of the SNUs into nascent fibrils resembling a string of beads (step 2). The protofibrils may stretch and tilt to the left or to the right (as seen in Fig. 3a and 3b). The next stage is characterized by the merging and stretching of fibrils and their transformation into striated ribbons (step 3). This is followed by their further evolution to form MSRs and RCDs (steps 4 and 5). MSRs and RCDs may reflect different arrangements of their strands, and variations in these arrangements, including the degree of strand stretching, twisting and/or association, may account for tau fibrils that assume the morphologies of SFs, PHFs, TRs. Fibrils of different morphology may be inter-convertible depending on conditions in the microenvironment (steps 6 to 11).